Title: Autophagy regulates ARF7 degradation to facilitate root branching

Running title: Autophagy modulates root branching

Ebstrup E[1+], Ansbøl J[1+], Chevalier J[1],Clemmens P[1], Rodriguez E[1*]

[1]Innate immunity and cellular reprogramming group. Functional Genomic section, Department of Biology, University of Copenhagen, Denmark.

[+]These authors contributed equally to this work

*Correspondence to: Eleazar.rodriguez@bio.ku.dk

Abstract

Auxin orchestrates growth and developmental regulation in plants. For instance, auxin dictates root architecture via the Auxin Response Factor (ARF) family of transcription factors, which control lateral roots (LR) formation. In *Arabidopsis*, ARF7 is essential for the correct definition of LR's prebranch sites (PBS) through gene expression oscillation and plays a pivotal role during LR initiation. Despite ARF7's importance to this process, there is a surprising lack of knowledge about how ARF7's turnover is regulated and its role during root architecture patterning. Here, we show that ARF7 accumulates in autophagy mutants, localizes to autophagosomes and it's targeted for degradation through NBR1-dependent selective autophagy. Moreover, the rhythmic changes to ARF7 abundance are a whole plant process and require autophagy to occur. Surprisingly, autophagy deficiency does not seem to impact PBS establishment but affects LR formation; this might be explained because autophagy's regulation of ARF7 abundance mainly occurs in mature tissue. In conclusion we report a novel role for autophagy during plant development, through the selective degradation of ARF7 to optimize root branching.

Introduction

The plant root system plays a fundamental role as a point of contact with the plant's surroundings and allows adaptation to multiple stresses. Contrary to primary roots, lateral root (LR) development is post embryonic, which means that LR architecture is heavily influenced by growth conditions (Lv *et al*, 2021). As LR growth is modular, perception of the correct developmental conditions authorizes the repetition of LR modules along the primary root, maximizing the root's surface area. LRs originate from a cell layer called pericycle which surrounds the vasculature, and occurs sequentially in 4 steps: positioning, initiation, outgrowth, and emergence. During the positioning step, the plant ensures the spatiotemporal distribution, priming and activation of LR founder cells (LRFC) (Du & Scheres, 2018). LR spacing is controlled by an oscillatory root clock which dictates gene expression and cycles every 4-6h (Moreno-Risueno *et al*, 2010, 2015; Wachsman *et al*, 2020). This oscillatory clock is regulated (among others) by the phytohormone auxin and can be characterized through monitoring of reporter markers under the control of DR5, a synthetic promoter containing tandem repeats of an auxin responsive TGTCTC element (Ulmasov *et al*, 1997). DR5 expression analyses lead to definition of 2 contrasting oscillation phases: in-phase (concurrent with DR5 maximum signal) and anti-phase (DR5 minimum signal) which reciprocally repress each other (Moreno-Risueno *et al*, 2010). One of the genes displaying anti-phase expression is AUXIN RESPONSIVE FACTOR 7 (*ARF7*), a key transcription factor (TF) which regulates LR formation (Okushima *et al,* 2007). Importantly, analysis of *ARF7* loss of function mutant (Moreno-Risueno *et al*, 2010) indicates that this TF's oscillation is essential for the correct establishment of LR pre branch sites (PBS).

While positioning and initiation are broadly regulated by different mechanisms, ARF7 and its 2 TF targets LATERAL ORGAN BOUNDARIES DOMAIN (LBD) 16 and LBD33 are among the few genes that participate in both processes (Moreno-Risueno *et al*, 2010), which again attest to the pivotal role of ARF7 during LR formation. During the initiation step, the auxin signalling node IAA14-ARF7-ARF19 controls LBD16 activation in the LRFC, which is necessary to achieve asymmetry and initiate cell division (Goh *et al*, 2019). In addition to the importance of *ARF7* transcriptional oscillation for LR formation, it has also been shown that the subcellular localization of ARF7 is important for its function: nuclear localization correlates with auxin responsive tissue while in less responsive areas, activating ARFs concentrate to form cytoplasmic foci with liquid-like and solid-like proprieties (Powers *et al*, 2019). This body of evidence demonstrate the complexity necessary to correctly regulate ARFs-dependent responses, as an intricate web of processes are balanced to tightly regulate ARFs levels and compartmentalization. Yet surprisingly, little is known about how proteostasis mechanisms manage ARF7 and how this impacts the cellular decision making behind LR formation authorization.

Macroautophagy (herein autophagy) is an evolutionary conserved catabolic process which partakes in cellular recycling of macromolecules and organelles (Levine & Klionsky, 2004). Autophagy is

characterized by the formation of an isolation membrane enclosing a portion of cytoplasm to form a double-membraned vesicle termed the autophagosome. Firstly, characterized during starvation stress, autophagy was viewed as a random process due to the observation of what seemed to be an indiscriminate engulfment of portions of the cytoplasm. Further studies unveiled the existence of several selective cargo adaptors which allow for targeted degradation of cellular constituents (*e.g.,* Svenning *et al*, 2011; Nolan *et al*, 2017; Stephani *et al*, 2020; Wu *et al*, 2021), meaning that autophagy can be highly selective and participate in targeted remodelling of the cell. Perhaps one of the most characterized cargo receptors in plants is NEIGHBOUR OF BRCA1 (NBR1, Svenning *et al*, 2011), a hybrid of mammalian *NBR1* and *p62*, possessing a PB1 domain necessary for homopolymerization and biomolecular condensate formation and an UBA domain for ubiquitin binding. It is through the latter that NBR1 binds ubiquitinated cargo which are then targeted for autophagic degradation via NBR1's interaction with the autophagosome decorating proteins ATG8s (*e.g.,* Zhou *et al*, 2013; Zhou *et al*, 2014; Hafrén *et al*, 2017; Ji *et al*, 2020; Tarnowski *et al*, 2020). The ability to function selectively allows autophagy to participate in a variety of stress responses, namely by promoting the cellular reprogramming necessary to enact appropriated responses (Rodriguez *et al*, 2020). Without surprise, autophagic deficiency have been shown to cause myriads of developmental defects; interference with core autophagic machinery component often causes lethality during early developmental stages, severe developmental defects, and shortened life span in metazoans (*e.g.,* Scott *et al*, 2004; Liu *et al*, 2015; Yoshii *et al*, 2016). In contrast, plants are able to tolerate disruption of autophagy activity without major penalties: autophagy deficient mutants display subtle growth phenotypes like reduced biomass and inflorescence numbers, and premature senescence (Bassham *et al*, 2006), but importantly, are able to complete their life cycle and generate fertile progeny. It thus seems that the phenotypic "struggles" of plant *atg* mutants become more apparent under stressed conditions, as can be attested by the many publications linking autophagy with stress responses (*e.g.,* Liu *et al*, 2009; Hofius *et al*, 2009; Vanhee *et al*, 2011; Zhou *et al*, 2013; Munch *et al*, 2014; Chen *et al*, 2015; Nolan *et al*, 2017; Sedaghatmehr *et al*, 2019; Rodriguez *et al*, 2020). For instance, autophagy has been shown to be involved in primary root growth and LR formation during nutrient starvation (Deb *et al*, 2014; Huang *et al*, 2019), which is consistent with the cross-kingdom descriptions of the starvation-alleviating properties of autophagy (Scott *et al*, 2004; Desideri *et al*, 2012; Huang *et al*, 2015; Wu *et al*, 2021). In contrast, the role of autophagy in regulating root architecture under normal developmental conditions is less understood.

In this work, we explored the contribution of autophagy in mediating ARF7's dependent responses. By using a combination of cell imaging and biochemical, genetics and molecular biology approaches, we demonstrate that ARF7's turnover is processed via NBR1-mediated selective autophagy. Importantly, we demonstrate that ARF7's abundance rhythmically oscillates in the whole plant and autophagy is necessary for proper establishment of ARF7's rhythm. Surprisingly, our data indicates that autophagy mutants display normal PBS establishment but have reduced LR formation, and together with ARF7 x

ATG8 co-localization experiments, suggest that ARF7 might be regulated by different mechanisms in a tissue specific manner. With these findings, we reveal an important regulatory role for selective autophagy during auxin responses through the turnover of the important auxin signalling regulator ARF7 and consequent fine-tuning of root architecture.

Results

Autophagy modulates ARFs *turnover.*

We have recently reported that autophagy participates in stem cell reprogramming and differentiation in the distantly related species *P. patens* and *A. thaliana* (Rodriguez *et al*, 2020; Kanne *et al*, 2021). Because *Arabidopsis* stem cell formation executes a program similar to LR formation (Sugimoto *et al*, 2010), we wondered if key regulators of these processes might be modulated via autophagy. As seen in Fig 1, ARF7 accumulates in different autophagy mutants (Fig 1A & B) and in the KO of the autophagic cargo adaptor NBR1 (Fig 1C), when compared to Col-0. *ARF7* relative expression was around 30% lower in *atg* mutants than Col-0 (Fig 1D), ruling out enhanced *ARF7* transcription as the source for ARF7 accumulation in *atg* mutants. To address if ARF7 accumulates exclusively due to autophagy deficiency, we also treated seedlings with the proteasome inhibitor with MG132 (Fig 1A-C) and observed that simultaneous inhibition of both degradation pathways leads to further accumulation of ARF7. These results indicate that ARF7 proteostasis is dependent on autophagy and the proteasome and are in agreement with data by Jing *et al*, (2022), in what concerns proteasomal participation in ARFs turnover. Because ARF7 often works together with ARF19 during regulation of root architecture, we also enquired about autophagy's role during ARF19 turnover. Immunoblot probing of pARF19::ARF19-GFP/*nph4-1 arf19-1* seedlings (Okushima *et al*, 2007) treated with or without the vacuolar protease inhibitors Pepstatin A and E-64D for 24h (Fig EV1) revealed substantial accumulation of ARF19-GFP when vacuolar proteases were inhibited. Together, these results indicating that autophagy participates in the turnover of these essential LR formation regulators.

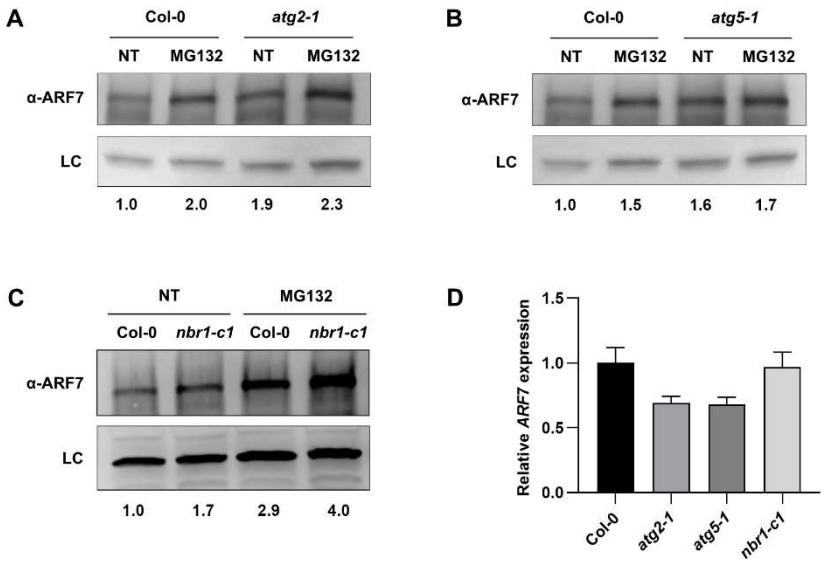

Figure 1*:* ARF7 is degraded via autophagy. **A-C**) ARF7 immunoblots in Col-0 and **a)** *atg2-1*; **b)** *atg5-1*; **c)** *nbr1-c1* with or without addition of the proteasomal inhibitor MG132. Values below each band represent the ratio between ARF7 and the loading control (LC) normalized to untreated Col-0 (NT), which was set to 1. **D**) *ARF7* relative expression in given genotypes. *ARF7* expression was normalized to *Actin2* and is relative to Col-0 (set to 1). Results provided in Figs A-D are representative of 3 biological replicates.

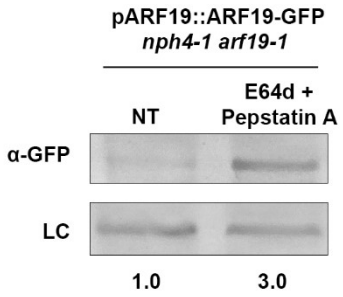

Fig EV1*:* Autophagy inhibition promotes ARF19 accumulation. GFP immunoblot of 14-day-old pARF19::ARF19-GFP/*nph4-1 arf19-1* seedlings grown in MS or MS supplemented with vacuolar protease inhibitors E-64D and Pepstatin A for 24h. Values below each band represent the ratio between ARF19-GFP and the loading control (LC) normalized to untreated (NT), which was set to 1. Image is representative of 3 biological replicates.

ARF7 *interacts with* NBR1 *and* ATG8a *in planta*

To further substantiate our claim that autophagy participates in the targeted degradation of ARF7 we performed protein-protein interaction studies. For this purpose, we used *Arabidopsis* stable transgenic lines expressing ARF7-Venus under the control of its native promoter (*pARF7::gARF7-Venus* herein called *ARF7-Venus,* Orosa-Puente *et al*, 2018) and performed coimmunoprecipitation (Co-IP) experiments. The experiment revealed that both NBR1 (Fig 2A) and ATG8a (Fig 2B), but not free YFP, co-immunoprecipitated with ARF7-Venus. Moreover, a web-based analysis (http://repeat.biol.ucy.ac.cy/iLIR; Jacomin *et al*, 2016) identified several potential ATG8-interaction

motifs (AIM) in ARF7, supporting our findings. As a cautionary note, we were unable to detect ARF7-Venus in the input of both Co-IPs which can likely be explained by the fact that ARF7-Venus is under the control of its native promoter and thus lowly expressed. In this line, we also performed Bimolecular fluorescence complementation (BiFC) analysis with a system allowing simultaneous, multi-protein interaction studies (Gehl *et al*, 2009) to transiently expressed Venus^{N}-ARF7 with SCFP^{N}-ATG8a and either SCFP^{C}-NBR1 or SCFP^{C}-TSPO, (TRYPTOPHAN-RICH SENSORY PROTEIN, an autophagic cargo adaptor for aquaporins, Hachez *et al*, 2014) in *Nicotiana benthamiana* leaves. As expected, SCFP^{C}-NBR1 and SCFP^{N}-ATG8a were able to reconstitute CFP to produce distinct signal localized in the nuclei and cytoplasm (Fig 2C). Moreover, Venus^{N}-ARF7 and SCFP^{C}-NBR1 produced GFP signal, which was localized to the cytoplasm and nuclei, in many instances co-localizing with NBR1-ATG8a CFP signal (Fig 2C). In contrast, SCFP^{C}-TSPO did not produce GFP signal when co-expressed with Venus^{N}-ARF7. In combination, these results indicate that ARF7 interacts with autophagic components and cumulative with data from Fig 1, indicates that this TF is degraded via NBR1-mediated selective autophagy.

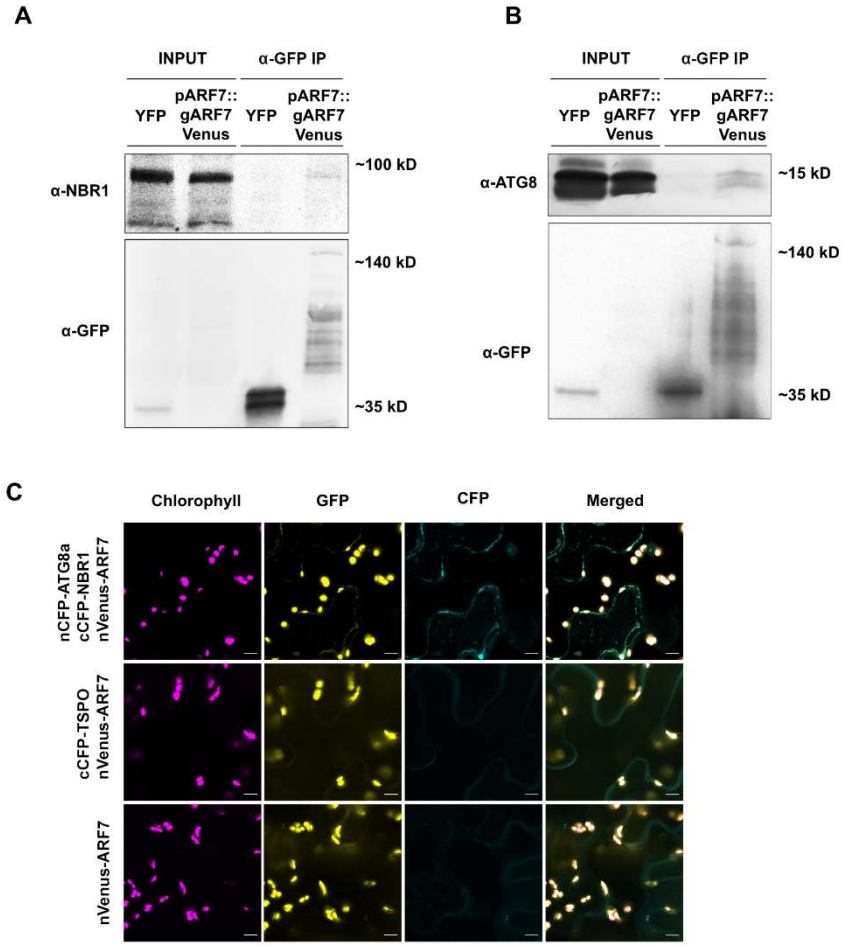

Figure 2 ARF7 associates with autophagic components NBR1 and ATG8a. **A, B)** ARF7 and ATG8/NBR1 association was tested by Coimmunoprecipitation (Co-IP) assay. Protein extracted from *Arabidopsis* lines expressing *pARF7::gARF7-Venus* or free *YFP* were immunoprecipitated with anti-GFP antibody and subsequently probed with antibodies raised against NBR1

or ATG8a. **C**) Bimolecular fluorescence complementation experiment shows oligomerization of ARF7, NBR1 and ATG8a in *N. Benthamiana*. Images were taken 48 hpi. cCFP-TSPO was used as control. Scale bar: 10 µM

ARF7 co-localization with autophagosomes follows a daily rhythm and is triggered by auxin.

Having established that autophagy regulates ARF7 abundance, it should be likely that this TF should co-localize with autophagosome-like structures. To assess this, we crossed ARF7-Venus to mCherry-ATG8a or mCherry-NBR1 reporter lines (Svenning *et al*, 2011) and used this for live cell imaging. As expected, both autophagy-related proteins localized to cytoplasmic punctae, in many instances co-localizing with ARF7-Venus. Moreover, mCherry-ATG8a also co-localized with ARF7-Venus in the nucleus (Fig 3 & Fig EV2). It should be noted that the co-localization of ATG proteins with ARF7 in cytoplasmic foci is mainly observable in the root's maturation zone while in younger tissue ARF7 primarily localizes in the nucleus (Fig EV2); this is in agreement with previous reports demonstrating that ARF7 partitioning is dependent on developmental stage of the tissue (Powers *et al*, 2019; Orosa-Puente *et al*, 2018).

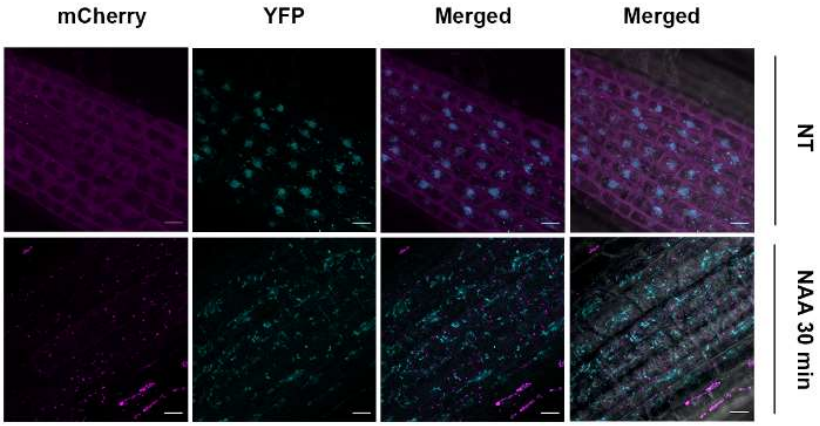

Figure EV2 NAA increases ARF7 condensation in the root tip. pARF7::gARF7-Venus x mCherry-ATG8a plants were treated with MS or MS supplemented with 1 µM NAA for 30 min. Scale bar 10 µM.

ARF7's nucleo-cytopartitioning has been ascribed to liquid-liquid phase separation (LLPS) to form cytoplasmic condensates (Powers *et al*, 2019); likewise, autophagosome formation sites and protein cargo triage (Kirkin *et al*, 2009; Zhang *et al*, 2009; Fujioka *et al*, 2020) are also dependent on LLPS. To address the nature of these cytoplasmic ARF7 & ATG8 foci, we incubated seedlings expressing mCherry-ATG8 and ARF7-Venus with the LLPS inhibitor 1,6-hexanediol (Wang *et al*, 2021; Xie *et al*, 2021) and tracked the stability of those foci over time. Most of the foci in which ARF7-Venus and mCherry-ATG8a co-localized were sensitive to 1,6-hexanediol treatment (Fig EV3), suggesting that these structures have liquid-like properties. Interestingly, some of these co-localizing events were insensitive to 1,6-hexanediol treatment, even after prolonged exposure (*i.e.,* more than 30 min),

indicating that those assembles have solid-like properties. Our data is both in agreement with findings for ARF7 (Powers *et al*, 2019) and studies in mammalians showing that NBR1 (and p62) is involved in condensate formation during autophagic degradation of substrates (Turco *et al*, 2021).

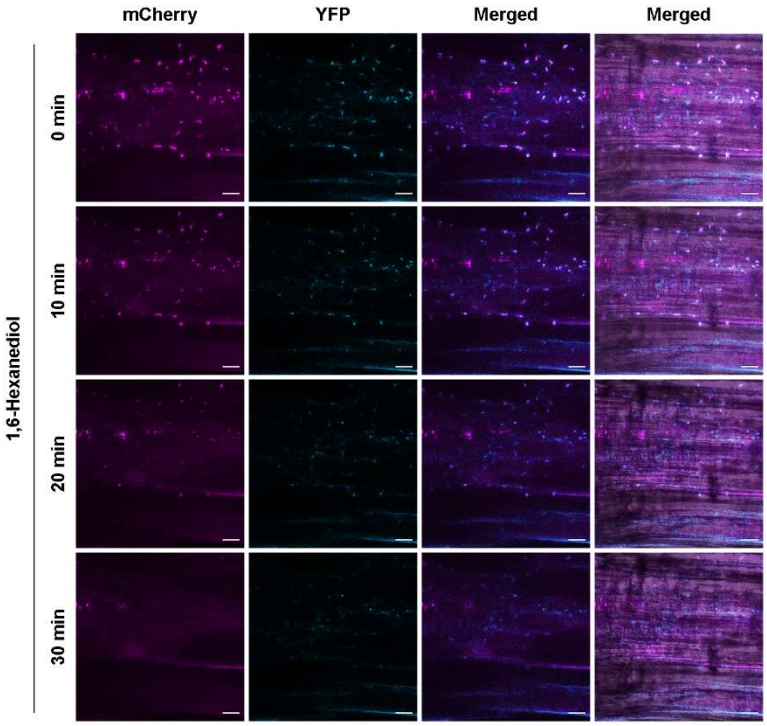

Figure EV3 ARF7 and ATG8 condensates have both liquid and solid properties. *pARF7::gARF7-Venus* x mCherry ATG8a plants were treated with 1,6-Hexanediol and imaged at given time points. Representative pictures were taken in the differentiation zone of 10–14-day old *Arabidopsis* seedlings. Leftmost Merge column represent the merger of YFP and mCherry channels, while the rightmost also includes the T-PMT channel (Brightfield) Scale bar 10 µM.

While our data demonstrates that autophagy plays a clear role in controlling ARF7's abundance, which conditions/factors trigger ARF7 turnover are unclear. To tackle this, we decided to treat our double reporter line with auxin or cytokinin treatment; our rationale being two-fold: a) auxin and cytokinin often act in contrast to each other during many developmental processes (Du & Scheres 2018); b) we have recently shown that plants rapidly engage autophagy to remodel the proteome upon perception of wide range of treatments, among them auxin and cytokinin (Rodriguez *et al*, 2020). We started by imaging the maturation zone, as ARF7 cytoplasmic condensates are mostly observed in this region. We noticed that the co-localization of ARF7-Venus with mcherry-ATG8a varied during the time of the day, *i.e.,* there is a significant increase (45% to 85%, $P<0.05$) in ARF7 and ATG8a co-localization when comparing seedlings imaged during zeitberg time (ZT, time after the lights are switched on) ZT0 vs ZT6, respectively. This is consistent with previous reports (Perianez-Rodriguez *et al*, 2021) showing that ARF7 expression follows a periodic fluctuation of 4-6h in the oscillation zone. Given this, we

decided to use ZT0 as the timepoint for subsequent treatments. Next, we incubated seedlings with vacuolar protease inhibitors (Pepstatin A and E-64d); this led to a dramatic increase in ARF7-Venus co-localization with mChery-ATG8a (Fig 3B & C) again supporting the proposition that ARF7 condensate formation can be linked to autophagic degradation. Similarly, NAA treatment promoted a significant increase of ARF7-Venus co-localization with mCherry-ATG8 positive punctae in the cytoplasm (Fig 3B & C) while Kinetin did not lead to increased ARF7-Venus co-localization with mCherry-ATG8a (P>0.05). Altogether, our results suggest that ARF7 cytoplasmic localization might be part of a proteome remodelling strategy which is mediated, at least in part, via autophagy.

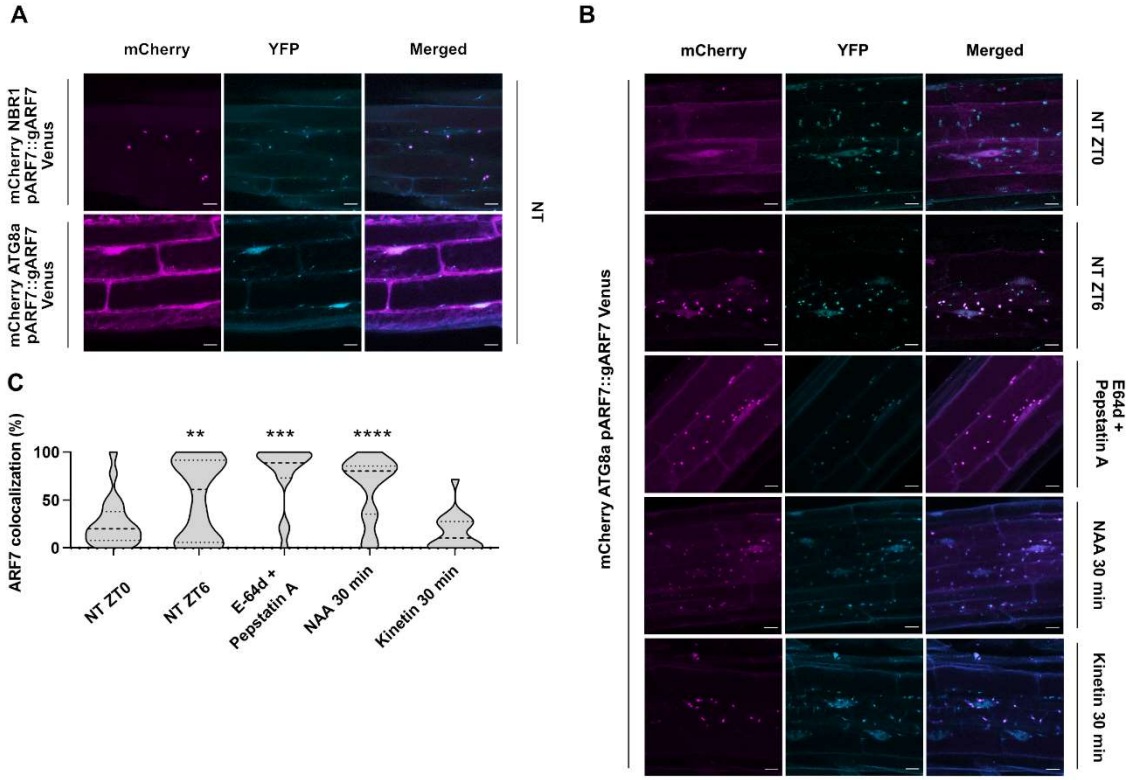

Figure 3 ARF7 co-localization with autophagosomes displays rhythmic variation and is enhanced by NAA treatment. **A**) Co-localization of ARF7-Venus with mCherry-ATG8a (Nuclei and/or cytoplasmic foci) or mCherry-NBR1 (cytoplasmic foci). Representative pictures were taken in the differentiation zone of 10–14-day old *Arabidopsis* seedlings. Scale bar 10 µM. **B)** ARF7-Venus co-localization with autophagosomes under selected treatments: No Treatment (NT), E64d + Pepstatin A (vacuolar protease inhibitors), NAA (1µM NAA for 30 min) and Kinetin (1µM Kinetin for 30 min). Scale bar 10 µM. **C)** Quantification of the co-localization of ARF7-Venus with mCherry-ATG8a under conditions depicted in **B)**. The outline of the violin plots represents the probability of the kernel density. Dotted lines represent interquartile ranges (IQR), with the thick horizontal line representing the median; whiskers extend to the highest and lowest data point. Results were obtained from three independent experiments with at least 6 plants per condition, asterisks mark statistical significance to NT according to a Wilcoxon signed-rank test (*P < 0.01; **P < 0.001).

Autophagy regulates rhythmic changes to ARF7 protein abundance but is not required for PBS establishment

Intrigued by our results showing that co-localization between ARF7 and ATG8a follows rhythmic variation and knowing that *ARF7* expression also shows a similar pattern in the OZ (Perianez-Rodriguez *et al*, 2021), we decided to explore the impact of autophagy in the natural variation of ARF7's abundance. Therefore, we performed immunoblots against ARF7 in Col-0 and *atg* mutants' seedlings during a 12h period. As it can be seen in Fig 4A, ARF7 levels increased from ZT0 to ZT6, followed by progressive decline up to ZT12, which is in agreement with the abovementioned pattern for *ARF7* transcript oscillation in the OZ. Moreover, these results likely explain the variation in co-localization of ARF7-Venus with autophagosomes at different timepoints (Fig 3): condensation is dependent on target concentration (Mcswiggen *et al*, 2019) and therefore more likely observable under high ARF7 levels (ZT6). Our findings also illustrate that ARF7 abundance display rhythmic changes in the whole plant, which is consistent *ARF7*'s expression profile (*e.g.,* Rosado *et al*, 2012; Lee *et al*, 2019) and with ARF7's role during hypocotyl gravi- and phototropism (Wang *et al*, 2020).

In marked contrast, the rhythmic variation in ARF7's abundance was lost when autophagy was disrupted (Fig 4B-D). Moreover, the transcript levels of *LBD16*, which is directly regulated by ARF7s, also lost its rhythmic fluctuation in *atg* mutants (Fig 4E). Interestingly, *LBD16* levels are significantly higher in *atg2-1* than Col-0, which could be related to the overall higher levels of ARF7 seen in *atg* mutants. Taken together, these results demonstrate the importance of autophagy in regulating ARF7-dependent rhythm.

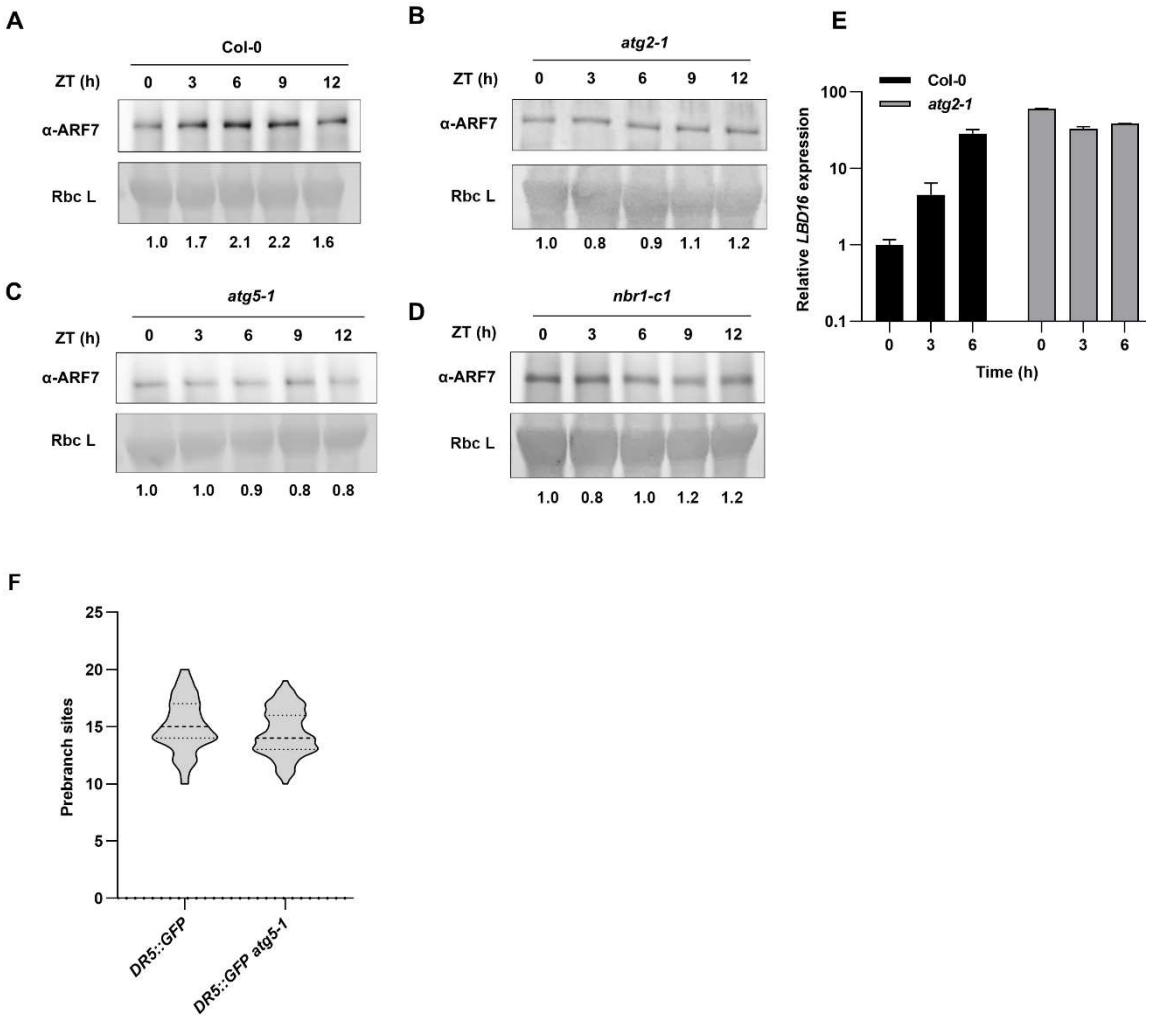

Figure 4: ARF7 abundance displays whole-plant rhythmic variation and is modulated by autophagy. **A-D)** ARF7 immunoblots from proteins extracted from Col-0 (**A**); *atg2-1* (**B**); *atg5-1* (**C**) or *nbr1-c1* (**D**) at given zeitberg time (ZT0-ZT12). Values below each band represent the ratio between ARF7 and RuBisCO large subunit (Rbc L) in respect to untreated Col-0 (NT), which was set to 1. Experiments were repeated at least 3 times with similar results. **E)** Relative gene expression oscillation of *LBD16* in Col-0 and *atg2-1* at given timepoints. *LBD16* expression was normalized to *ACTIN2* and set to 1 for each genotype at timepoint 0h.**F)** Pre Branch Site (PBS) in *DR5::GFP* and *DR5::GFP x atg5-1*. PBS of 5-day post germination, vertically grown seedlings were scored with a stereo microscope. The outline of the violin plots represents the probability of the kernel density. Dotted lines represent interquartile ranges (IQR), with the thick horizontal line representing the median; whiskers extend to the highest and lowest data point. Results were obtained from 4 independent experiments with a total of at least 80 plants per genotype.

ARF7 oscillation has been established as an essential step during PBS determination as *arf7-1* mutants display abnormal PBS patterning (Perianez-Rodriguez *et al*, 2021). Because ARF7 abundance does not seem to change when autophagy is impaired, we questioned whether PBS establishment could be affected in *atg* mutants. To track this, we compared PBS numbers in Col-0 and *atg5-1* lines expressing *DR5::GFP* with a stereo microscope. As seen in Fig 4F, there was no major differences in PBS count (P>0.05) between both genotypes, being that total PBS numbers we report are comparable to those

available in the literature for Col-0 (Moreno Risueno *et al*, 2010). This indicates that defective autophagy does not interfere with PBS establishment, despite affecting ARF7 turnover. Intriguingly, our results could also suggest that ARF7 oscillation might not be necessary for PBS establishment, which is in contrast to previous reports (Perianez-Rodriguez *et al*, 2021). Several explanations could justify these seemingly contradictory differences. Firstly, *ARF7*'s oscillation relevance during PBS establishment was inferred from analysing *arf7-1*, in which the oscillation is lost due to ARF7 absence. Contrastingly, oscillation of ARF7 is lost in *atg* mutants but the protein is still expressed; it is thus possible that while ARF7 is undoubtedly important for correct PBS establishment, the oscillation of this protein is not essential for the process. Alternatively, the oscillatory nature of *ARF7* as part of the root clock in the OZ might be under different regulatory processes than in the rest of the plant. To analyse this, we decided to revisit the co-localization between ARF7 and ATG8a but this time focusing on the younger root tissue (meristematic/elongation zones). In these zones, ARF7 mainly localize in the nuclei so opportunities for co-localization with ATG8a are seldom (Fig EV3). Because NAA treatment induces co-localization between ARF7 and ATG8 in the maturation zone (Fig 3), we repeated this procedure focusing now on the root tip. Remarkably, ARF7-Venus cytoplasmic signal was substantially increased by NAA treatment (Fig EV3), with many cytoplasmic foci being observable under this condition. mCherry-ATG8 punctae also increased dramatically, which is consistent with our previous reports showing that quick bursts of auxin lead to rapid autophagic activation (Rodriguez *et al*, 2020); but surprisingly, instances of co-localization with ARF7-Venus were still scarce (Fig EV3) despite the massive increase in both ARF7 and ATG8 positive foci. These results suggest that autophagic regulation of ARF7 abundance might be tissue-specific. Recent findings (Llamas *et al*, 2021), show that root meristem has tissue specific mechanisms (*i.e.* high chaperonin expression) to prevent protein aggregation and maintain stemness, which is consistent with the known role of NBR1 during aggrephagy (*e.g.*, Jung *et al,* 2020) and with our proposition that autophagic turnover of ARF7 occurs mainly in mature tissue.

Given that NAA induced ARF7's localization to cytoplasmic foci, we wondered if a rapid NAA treatment had any effect in ARF7 abundance. Hence, we immunoblotted ARF7 in Col-0 and *atg5-1* seedlings treated with NAA for 30 min at ZT0 and ZT6 (Fig EV4). The results indicate that Col-0 seedlings responded to NAA by accumulating ARF7 and interestingly, ARF7 reached higher levels at ZT6 than ZT0 (roughly 2-fold higher). This is consistent with the increased co-localization of ARF7 and ATG8a at ZT6 (Figure 3) as condensation should be enhanced by increased abundance of ARF7. In combination, our results also suggests that this condensation mechanism might be part of a strategy to keep ARF7 levels in check, preventing excessive nuclear ARF7 and consequent exaggerated auxin responsiveness. In contrast to previous reports (e.g., Wang *et al*, 2005; Perianez-Rodriguez *et al*, 2021), our data suggest that auxin treatment induces changes to ARF7 abundance. These differences might be easily conciliated due to different experimental set ups among reports: longer auxin treatments (3h-16h)

and different tissues (e.g., protoplast or only the root's OZ) were used in those reports as opposed to the experimental setup used here. This is supported by our data, which indicates that tissue specific mechanisms and time of the day seem to be important factors during ARF7 turnover and also by predicted buffering mechanisms of ARF7 signalling (Perianez-Rodriguez 2021). Concerning *atg5-1* seedlings, NAA treatment did not lead to ARF7 accumulation at any of the timepoints tested (Figure 4) which which might not be surprising given that ARF7 levels are already elevated when autophagy is impaired and that other mechanisms (*e.g.*, proteasome) might be upregulated during auxin perception to compensate for defective autophagy. In sum, these experiments reveal that while the oscillation of ARF7 abundance seems to be a whole plant phenomenon, the means by which this regulation occurs might be tissue specific, with autophagy playing a more prominent role in mature tissue but only a minor role in younger tissue. Likewise, this apparent tissue-specific regulation of ARF7 turnover also reconciles our findings with those of Perianez-Rodriguez *et al*, (2021), about the relevance of *ARF7* oscillation to PBS establishment and justifying normal PBS establishment in *atg* mutants.

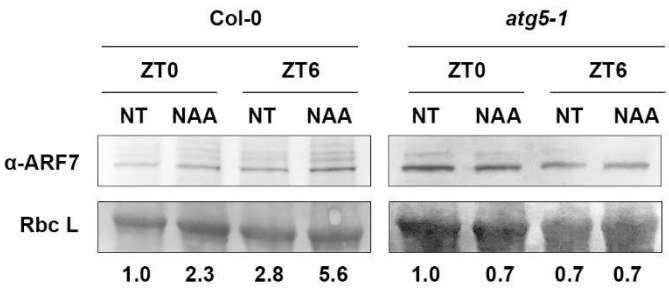

Figure EV4 NAA-induced changes to ARF7's abundance is lost in *atg* mutant. ARF7 immunoblot from proteins extracted from Col-0 or *atg5-1* treated with MS or MS supplemented with NAA (1µM, 30 min), at zeitberg time 0 (ZT0) or zeitberg time 6 (ZT6). Values below each band represent the ratio between ARF7 and the loading control (Rbc L), relative to untreated sample (NT), which was set to 1. Experiments were repeated at least 3 times with similar results.

Autophagy facilitates LR formation

As our results suggest that autophagy's contribution to ARF7 turnover might be more prominent in mature tissue, we wondered if accumulation of ARF7 in *atg* mutants could have an impact in other ARF7-dependent phenotypes. Besides PBS, ARF7 regulatory role during LR initiation is also well established (*e.g.,* Okushima *et al*, 2007; Goh *et al*, 2019); consequently, we examined *atg* mutant's ability to produce LRs by transplanting 3-day old seedlings to vertical plates and scored LRs after 7 days. As shown in Fig 5, *atg* mutants have a significantly lower LR density when compared to Col-0. Because we have seen that lack of autophagy leads to condensation of ARF7 (Fig 3 and Fig EV2) which has been linked with decreased auxin responses (Powers et al 2019) and also because NAA treatment did not produce major changes to ARF7 abundance in *atg5-1* seedlings, we questioned if *atg* mutants might have dampened auxin responses. To ascertain this, we germinated Col-0 and *atg* mutants and

after 5 days, transferred them to vertical MS plates with or without NAA (0.1 µM) and counted LRs 9 days after germination. As seen in Fig 5 A & B, NAA treatment caused an increase in LR density for all genotypes, but it did not rescue the differences observed between Col-0 and *atg* mutants. These results are in agreement with our previous findings (Rodriguez *et al*, 2020) regarding *atg* mutants' reduced ability to respond effectively to callus inducing media (rich in auxin) to form callus, a process resembling LR initiation.

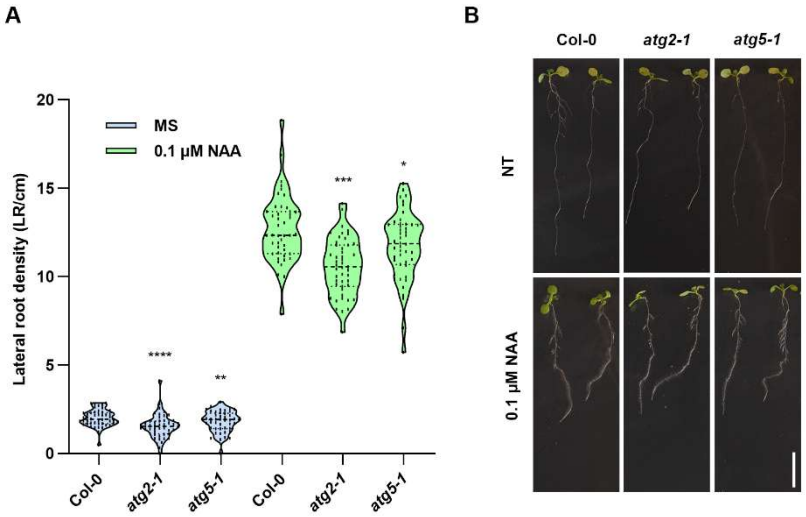

Figure 5 Autophagy deficient mutants have reduced LR formation capacity. The outline of the violin plots represents the probability of the kernel density. Dotted lines represent interquartile ranges (IQR), with the thick horizontal line representing the median; whiskers extend to the highest and lowest data point but no more than ±1.5 times the IQR from the box. Results were obtained from three independent experiments with at least 20 plants per condition, asterisks mark statistical significance to NT according to the t-test (*P < 0.01; ** P < 0.001; ****P < 0.0001; ****P < 0.00001). Scale bar: 1 cm

Discussion

Here, we show how autophagy modulates ARF7 and ARF19 turnover and this can be carried selectively through NBR1 (Fig 1 & 2). We and others (Jing *et al*, 2022) have shown that MG132 treatment also causes ARF7 to accumulate, which suggests proteasomal activity also regulates this TF turnover. However, care should be taken when inferring proteasomal contribution based solely on MG132-derived data as this inhibitor produces several off-target effects like transcriptional upregulation (Wang *et al*, 2008; Cho *et al*, 2013) and also interference with lysosomal proteases (Garrison & Bangs, 2020), and autophagosome assembly (Ji *et al*, 2016). Nonetheless, as we see a synergistic effect of MG132 and autophagy inhibition in ARF7 accumulation (Fig 1), it is likely that both degradation pathways are involved in regulating ARFs turnover. The recruitment of both degradation pathways to promote ARFs turnover is in line with the necessity to keep *ARF7* output under tight control (Moreno-Risueno *et al*,

2010; Perianez-Rodriguez *et al*, 2021) and also with the fact that excessive activating ARFs lead to dramatic developmental retardation due to exaggerated auxin program execution (Power et al 2019). Interestingly, we find that while *atg* mutants over accumulate ARF7, autophagy blockage leads to increased ARF7 cytoplasmic condensates, which have been linked to low responsiveness to auxin. Consequently, despite having higher ARF7 levels than Col-0, *atg* mutants show diminished auxin responses (Fig EV4), LR formation (Fig 5) and callus formation (Rodriguez et al 2020), a process reminiscent of LR initiation. How does accumulation of ARFs equate to diminished auxin responses? It is possible that autophagy inhibition leads to ARF7 accumulation which may induce supersaturation (Mcswiggen *et al*, 2019) and cause ARF7 condensation in the cytoplasm (Fig 1 & 3). Recent reports (Powers *et al*, 2019; Jing *et al*, 2022) have linked ARFs condensation with decreased auxin responsiveness, therefore, the disruption of protein degradation pathways we report here causes ARF7 levels to increase, promoting cytoplasmic aggregation and consequent reduced auxin responsiveness. While our data provides an indication that the mobilization of ARF7 to cytoplasmic foci might be part of a mechanisms aimed at adjusting ARF7 abundance and auxin responsiveness, more experiments are needed to fully understand this process. For instance, Jing *et al*, (2022) recently showed that the loss of function of AFF1 (F-box protein) displays reduced auxin responsiveness due to cytoplasmic hyper condensation and consequent nuclear depletion of ARFs. Despite these dramatic effects, the *aff1* mutants only display mild developmental phenotypes and even seems able to produce LRs when supplemented with 2-4D; this contrasts with *arf7 x arf19* mutant's severe LR formation defects, even when cultured with auxin (Okushima *et al*, 2007). Moreover, we report that ARF7 cytoplasmic foci do not co-localize with autophagosomes at the same extent in young vs mature tissues, even upon NAA treatment (Fig 3 and Fig EV2). While we cannot exclude that prolonged exposure to NAA could eventually enhance ARF7 and ATG8 co-localization in the OZ, it is evident that under short exposure, ARF7 cytoplasmic partitioning serves different functions depending on the tissue examined. Thus, the role of ARF's cytoplasmic localization in controlling ARFs abundance and signalling still needs further clarification.

Despite autophagy's role in modulating ARF7 abundance, PBS establishment do not seem to be affected when autophagy is defective (Fig 4). This could be explained both because in the OZ ARF7 is mainly localized in the nuclei (Powers *et al*, 2019) and autophagy seems to play a secondary role during ARF7s abundance regulation in this zone (Fig 3 & Fig EV2). However, we cannot rule out that autophagy does impact ARF7's oscillation in younger tissues, as we do see that ARF7-Venus can colocalize with ATG8a in the OZ, so further experiments are needed to fully answer this issue.

In contrast to PBS, LR formation seems to be impaired in *atg* mutants (Fig 5). In the context of LR formation, there is evidence of autophagic participation in a wide range of processes like cell death regulation of endodermal cells above LRPs (Escamez *et al*, 2020) and potentially also during PIN's degradation (Kleine-Vehn *et al*, 2008). Moreover, autophagy is also involved in the regulation of

proteome turnover triggered by other hormonal responses like ABA (Rodriguez *et al*, 2020) and cytokinin (Acheampong *et al*, 2020; Rodriguez *et al*, 2020) which are known to influence LR formation. For these reasons, deficiencies in such a transversal process like autophagy complicate result interpretation and ascribing phenotypes to a specific function of autophagy. For instance, ABA is known to interfere with LRs formation (de Smet *et al*, 2003) and consequently, misregulation of ABA signalling in *atg* mutants (Rodriguez *et al*, 2020) could be a source of defective LR formation. However, we have previously seen that *atg* mutants have difficulties forming callus (Rodriguez *et al*, 2020) a process resembling LR initiation and because ABA does not affect callogenesis (Sugimoto *et al*, 2010), it is plausible that LR deficiencies in *atg* mutants occur at an earlier stage than ABA-induced effects (LR emergence). Nonetheless, because our results unequivocally show that autophagy specifically impacts the turnover of the important LR regulators ARF7 and ARF19, it is undeniable that at the very least, defective ARFs turnover in *atg* mutants must contribute to the decreased auxin responses and LR formation we report here.

In conclusion, we have uncovered a novel role for selective autophagy during the turnover of the key developmental regulators ARF7 and ARF19 and provided further insight into the intricate mechanisms behind ARFs fine-tuning and how this affects root architecture.

Acknowledgements

This work was funded by a Danish Research Agency grant to E.R. (DFF1- 1032-00249B). We would like to thank Tom Guilfoyle (anti-ARF7 antibody), Koki Yoshimoto (anti-ATG8a antibody), Malcolm Bennett (pARF7::gARF7-Venus), Yasin Dagdas (*DR5::GFP* and *atg5-1 DR5::GFP*), Liwen Jiang (NBR1-C1) and Hidehiro Fukaki (pARF19::ARF19-GFP *nph4-1 arf19-1*) for sharing material/reagents. Thanks are also due to Miguel Moreno-Risueño and Nuria Coll for insightful discussion. We would also like to thank Suksawad Vongvisuttikun for technical assistance and the Plant Molecular Biology course 2022 class (University of Copenhagen, Denmark) for performing the ARF19-GFP western blot. Confocal microscopy imaging was performed using equipment from the Center for Advanced Bioimaging (CAB) Denmark, University of Copenhagen.

Author contributions

Conceptualization: ER; Investigation: ER, EE, JA, JC, PC. Formal analysis: ER, EE, JA. Writing: ER, EE, JA Visualization: ER, JA; Supervision: ER; Funding Acquisition ER. All authors read the manuscript and agreed with the findings reported

Methods and Materials

Plant material and phenotypic characterization

Arabidopsis seedlings were grown on solid, half-strength MS media (0.8% agar, 1% sucrose at 5.7 pH) and kept at 21 C° with a photoperiod of 16 h (120 µE/m^2/s). Seeds were sterilized with 1.3% bleach followed by 70% alcohol and then rinsed three times with sterilized water. The following lines were used throughout this study; Col-0, *atg2-1* (SALK_076727), *atg5-1* (SAIL_129_B07), *nbr1-c1* (Ji *et al*, 2020), mCherry ATG8a & mCherry NBR1 (Svenning *et al*, 2011), pARF7::gARF7 Venus (Orosa-Puente *et al*, 2018), pARF19::ARF19-GFP/*nph4-1 arf19-1* (Okushima *et al*, 2007), DR5::GFP and DR5::GFP *atg5-1* (Gift from Yasin Dagdas, GMI Vienna, Austria).

For the time course experiments, seedlings were acclimated in liquid half-strength MS media for at least 2 days before sampling. Sampling was done just before the chamber light was turned on ZT0, and then at indicated times. For LR and PBS scoring, seedlings were germinated on half-strength MS media and set to grow vertically for the indicated time, using a Leica M165 FC stereomicroscope. PBSs were counted after 7 days using GFP filter to visualize DR5 driven, GFP signal. Per genotype, at least 70 plants were analyzed derived from 6 independent experiments. LR's were counted at day 9, and only LR's that had at least reached stage IV were included. Per genotype/condition at least 40 plants were counted derived 6 independent experiment. All genotypes were blinded during counting in both assays to prevent potential bias.

Chemical treatments

For confocal microscopy and immunoblot assays, seedlings were acclimated in liquid half-strength MS media for 2 days acclimation before imaging. For hormone treatment effect on the co-localization of ARF7 with ATG8 & NBR1, samples were either treated with NAA (1 µM), Kinetin (1 µM), or MS for the given time. Chemical inhibition of autophagy was done by pre-treating seedlings with the vacuolar protease inhibitors E-64d (1:3000, stock 10 µM) and Pepstatin A (1 µM) 16 h prior imaging or western blotting. For inhibition of LLPS in the mature regions of the root, roots were imaged just before and directly after treatment with LLPS inhibitor 1,6-hexanediol (10%). Images were taken at 5 min interval for 30 min. Confocal imaging of the seedlings was taken with LSM700 Zeiss confocal microscope, at 20x or 63x water objective. Images were analyzed using Zen 2012 (Zeiss).

For protein analysis of ARF7 in *atg* mutants upon proteasomal blockage, samples were treated with or without MG132 (100 µM) for 16 h before harvest.

Protein extraction

Proteins were extracted using 3xSDS buffer (30% glycerol, 3% SDS, 94 nM Tris, pH 6.8, Bromophenol blue, Complete ultra-tablets EDTA-free protease inhibitor cocktail (Roche), 50mM DTT), then samples were centrifugated for 20 min at 4°C 14000 rpm and the supernatant was moved into a new tube. Samples were denatured at 95°C for 5 min before loaded it for SDS-PAGE.

SDS-PAGE and immunoblotting

Protein samples were separated on a 4-20% pre-casted gel (Bio-Rad) and transferred overnight onto nitrocellulose membrane (GE Healthcare). Membranes were blocked for 1 h with 5% skim milk (Merck) in TBST [50 mM Tris-HCL, pH 7.5 150 nM NaCl, 0.1% Tween-20 (Sigma)] and incubated 2 h at room temperature or overnight (4°C) with primary antibodies: anti-ARF7 (Wang et al, 2005)(Wang et al, 2005), anti-NBR1 (AS14 2805, Agrisera; 1:5000); anti-GFP (TP401 AMSBio, 1:1000); anti-ATG8a (Yoshimoto *et al*, 2004) Membranes were washed, followed by incubation in anti-rabbit HRP conjugate (Promega; 1:5000). Home-made chemiluminescent substrate (Mruk & Cheng, 2011) was applied before detection. Bands were quantified using ImageJ and normalized to loading controls.

Vector construction and Plant Transformation for BiFC

To create pDEST-ATG8a-SCYNE, pDEST-NBR1-SCYCE, pDEST-ARF7-VYNE and pDEST-TSPO-SCYCE, we PCR amplified (CloneAMP HIFI PCR premix, TAKARA) the coding sequences of *ATG8a*, *NBR1*, *ARF7 and TSPO* flanked recognition sequence for Gateway (Thermofischer) or In-Fusion (Clontech) cloning. *ATG8a, NBR1 and ARF7's* PCR products were cloned into pENTR (Life Technologies) and subsequentially transferred (LR clonase, Invitrogen) into the Gateway-compatible BiFC vectors (Gehl C *et al*, 2009) pDEST-^{GW} SCYNE, pDEST-^{GW}SCYCE, pDEST-^{GW}VYNE. *TSPO* PCR amplicon was directly cloned into pDEST-^{GW}SCYCE using In-Fusion cloning. *Agrobacterium* strain GV3101 containing constructs were grown in Yeast-extract peptone media supplied with the respective antibiotics overnight. Cultures were spun and resuspended in 10mM $MgCl_2$, 10 mM MES-K and 100 µM acetosyringone to the density of 600nm = 0.15-0.2 per construct and mixed 1:1 and left at room temperature for 2 h, followed by infiltration in 3 weeks old *N. Benthamiana*. Pictures were taken 48 hpi using a Zeiss LSM 700 confocal microscope.

Immunoprecipitation

Immunoprecipitation assay was described previously (Zuo *et al*, 2022). In brief, 1 g of 14-day old seedlings were grinded with mortar and pestle and 2 ml of IP extraction buffer (50mM Tris-HCl pH 7.5, 150mM NaCl, 5% glycerol 1mM EDTA, 0.1% NP40, 10mM DTT, protease inhibitor (mini

complete ultra, EDTA-free) was added, followed by centrifugation at 4°C 13000 rpm, 20 min. The supernatant was incubated with 20 µl GFP trap beads (Chromotek) rotating for 2-4-hours at 4°C. The beads were washed 3-4 times with washing buffer (20 mM Tris-HCl pH 7.5, 0.15 M NaCl, 0.1% NP40). 30 µL of 3xSDS was added to the beads and heat up 5 min at 95 °C before proceeding for SDS-PAGE.

RNA extraction

RNA was extracted as described previously (Zuo *et al*, 2022) using TRIzol reagent (Thermo Scientific), treated with DNase (Thermo Scientific) and was reverse transcribed into cDNA using Reverse Aid kit (Thermo Scientific) as described by the manufacturer. qPCR assays were executed on the Quantstudio 1 (Applied Biosystems) system using SYBR Green master mix (ThermoFisher), *ACT2* was used as internal control. All primers used for qPCR analysis are listed in Supplementary table 1. Experiment was repeated three times.

Supplementary table 1

Cloning primers	
ARF7 Forward primer	5'-CACCATGAAAGCTCCTTCATCAA-3'
ARF7 Reverse primer	5'-TCACCGGTTAAACGAAGTGGC-3'
NBR1 Forward primer	5'-CACCATGGAGTCTACTGCTA-3'
NBR1 Reverse primer	5'-TCAAGCCTCCTTCTCCCCT-3'
TSPO Forward primer	5'-GCAGGCTCCGCGGCCATGGATTCTCAGGACATCAGA-3'
TSPO Reverse primer	5'-AGCTGGGTCGGCGCGTCACGCGACTGCAAGCTTTAC-3'
ATG8a Forward	5'-CACCATGATCTTTGCTTGCTTGA-3'
ATG8a Reverse	5'-TCATCAAGCAACGGTAAGAGAT-3'
qPCR primers	
ACT2 Forward primer	5'-CTTGTTCCAGCCCTCGTTTGTG-3'
ACT2 Reverse primer	5'-CCTTGGAGATCCACATCTGCTG-3'
ARF7 Forward primer	5'-CAAGGTCACAGTGAGCAAGTCG -3'
ARF7 Reverse primer	5'-TGTGGAGCATGCATATGAGCTTGG -3'
LBD16 Forward primer	5'-TCCATGATCGATGTGAAGCTGTCG-3'
LBD16 Reverse primer	5'-TGTGATTGCAAGAAAGCCACCTG-3'

References

Acheampong AK, Shanks C, Cheng C-Y, Schaller GE, Dagdas Y & Kieber JJ (2020) EXO70D isoforms mediate selective autophagic degradation of type-A ARR proteins to regulate cytokinin sensitivity. *Proceedings of the National Academy of Sciences* 117: 27034–27043

Bassham DC, Laporte M, Marty F, Moriyasu Y, Ohsumi Y, Olsen LJ & Yoshimoto K (2006) Autophagy in development and stress responses of plants. *Autophagy* 2: 2–11

Chen L, Liao B, Qi H, Xie LJ, Huang L, Tan WJ, Zhai N, Yuan LB, Zhou Y, Yu LJ, *et al* (2015) Autophagy contributes to regulation of the hypoxia response during submergence in *Arabidopsis thaliana*. *Autophagy* 11: 2233–2246

Cho KS, Kwon KJ, Jeon SJ, Joo SH, Kim KC, Cheong JH, Bahn GH, Kim HY, Han SH, Shin CY, *et al* (2013) Transcriptional upregulation of Plasminogen Activator Inhibitor-1 in rat primary astrocytes by a proteasomal inhibitor MG132. *Biomolecules & Therapeutics* 21: 107

Deb S, Sankaranarayanan S, Wewala G, Widdup E & Samuel MA (2014) The S-domain receptor kinase *Arabidopsis* Receptor Kinase2 and the U Box/Armadillo repeat-containing E3 Ubiquitin Ligase9 module mediates lateral root development under phosphate starvation in *Arabidopsis*. *Plant Physiology* 165: 1647–1656

Desideri E, Filomeni G & Ciriolo MR (2012) Glutathione participates in the modulation of starvation-induced autophagy in carcinoma cells. *Autophagy* 8: 1769–1781

Du Y & Scheres B (2018) Lateral root formation and the multiple roles of auxin. *Journal of Experimental Botany* 69: 155–167

Escamez S, André D, Sztojka B, Bollhöner B, Hall H, Berthet B, Voß U, Lers A, Maizel A, Andersson M, *et al* (2020) Cell death in cells overlying lateral root primordia facilitates organ growth in *Arabidopsis*. *Current Biology* 30: 455-464.e7

Fujioka Y, Alam JM, Noshiro D, Mouri K, Ando T, Okada Y, May AI, Knorr RL, Suzuki K, Ohsumi Y, *et al* (2020) Phase separation organizes the site of autophagosome formation. *Nature* 578: 301–305

Garrison P & Bangs JD (2020) p97 inhibitor CB-5083 blocks ERAD in *Trypanosoma brucei*. *Molecular & Biochemical Parasitology* 239

Gehl C, Waadt R, Kudla J, Mendel R & Hansch R (2009) New GATEWAY vectors for high throughput analyses of protein-protein interactions by bimolecular fluorescence complementation. *Molecular Plant*: 1051–1058

Goh T, Toyokura K, Yamaguchi N, Okamoto Y, Uehara T, Kaneko S, Takebayashi Y, Kasahara H, Ikeyama Y, Okushima Y, *et al* (2019) Lateral root initiation requires the sequential induction of transcription factors LBD16 and PUCHI in *Arabidopsis* thaliana. *New Phytologist* 224: 749–760

Hachez C, Veljanovski V, Reinhardt H, Guillaumot D, Vanhee C, Chaumont F & Batoko H (2014) The *Arabidopsis* abiotic stress-induced TSPO-related protein reduces cell-surface expression of the aquaporin PIP2;7 through protein-protein interactions and autophagic degradation. *Plant Cell* 26:4974-90

Hafrén A, Macia J-L, Love AJ, Milner JJ, Drucker M & Hofius D (2017) Selective autophagy limits cauliflower mosaic virus infection by NBR1-mediated targeting of viral capsid protein and particles. *Proceedings of the National Academy of Sciences* 114: E2026–E2035

Hofius D, Schultz-Larsen T, Joensen J, Tsitsigiannis DI, Petersen NHTT, Mattsson O, Jørgensen LB, Jones JDGG, Mundy J & Petersen M (2009) Autophagic Components Contribute to Hypersensitive Cell Death in *Arabidopsis*. *Cell* 137: 773–783

Huang H, Kawamata T, Horie T, Tsugawa H, Nakayama Y, Ohsumi Y & Fukusaki E (2015) Bulk RNA degradation by nitrogen starvation-induced autophagy in yeast. *The EMBO Journal* 34: 154

Huang L, Yu LJ, Zhang X, Fan B, Wang FZ, Dai YS, Qi H, Zhou Y, Xie LJ & Xiao S (2019) Autophagy regulates glucose-mediated root meristem activity by modulating ROS production in *Arabidopsis*. *Autophagy* 15: 407–422

Jacomin AC, Samavedam S, Promponas V & Nezis IP (2016) iLIR database: A web resource for LIR motif-containing proteins in eukaryotes. *Autophagy* 12: 1945–1953

Ji C, Zhou J, Guo R, Lin Y, Kung C-H, Hu S, Ng WY, Zhuang X & Jiang L (2020) AtNBR1 is a selective autophagic receptor for AtExo70E2 in *Arabidopsis*. *Plant Physiology* 184: 777–791

Ji MM, Lee JM, Mon H, Xu J, Tatsuke T & Kusakabe T (2016) Proteasome inhibitor MG132 impairs autophagic flux through compromising formation of autophagosomes in *Bombyx* cells. *Biochemical and Biophysical Research Communications* 479: 690–696

Jing H, Korasick DA, Emenecker RJ, Morffy N, Wilkinson EG, Powers SK & Strader LC (2022) Regulation of AUXIN RESPONSE FACTOR condensation and nucleo-cytoplasmic partitioning. *Nature Communications 2022 13:1* 13: 1–11

Jung H, Lee HN, Marshall RS, Lomax AW, Yoon MJ, Kim J, Kim JH, Vierstra RD & Chung T. Arabidopsis cargo receptor NBR1 mediates selective autophagy of defective proteins. J Exp Bot. 2020 Jan 1;71(1):73-89.

Kanne J v., Ishikawa M, Bressendorff S, Ansbøl J, Hasebe M, Rodriguez E & Petersen M (2021) Overexpression of ATG8/LC3 enhances wound-induced somatic reprogramming in *Physcomitrium patens*. *Autophagy*: 1–4

Kirkin V, Lamark T, Sou YS, Bjørkøy G, Nunn JL, Bruun JA, Shvets E, McEwan DG, Clausen TH, Wild P, *et al* (2009) A role for NBR1 in autophagosomal degradation of ubiquitinated substrates. *Molecular Cell* 33: 505–516

Kleine-Vehn J, Leitner J, Zwiewka M, Sauer M, Abas L, Luschnig C & Friml J (2008) Differential degradation of PIN2 auxin efflux carrier by retromer-dependent vacuolar targeting. *Proceedings of the National Academy of Sciences of the USA* 105: 17812–17817

Lee HW, Cho C, Pandey SK, Park Y, Kim M-J & Kim J (2019) LBD16 and LBD18 acting downstream of ARF7 and ARF19 are involved in adventitious root formation in *Arabidopsis*. *BMC Plant Biology* 19: 1–11

Levine B & Klionsky DJ (2004) Development by Self-Digestion. *Developmental Cell* 6: 463–477

Liu EY, Xu N, O'Prey J, Lao LY, Joshi S, Long JS, O'Prey M, Croft DR, Beaumatin F, Baudot AD, *et al* (2015) Loss of autophagy causes a synthetic lethal deficiency in DNA repair. *Proceedings of the National Academy of Sciences* 112: 773–778

Liu Y, Xiong Y & Bassham DC (2009) Autophagy is required for tolerance of drought and salt stress in plants. *Autophagy* 5: 954–963

Llamas E, Torres-Montilla S, Lee H, Barja M, Schlimgen E, Dunken N, Wagle P, Werr W, Zuccaro A, Rodríguez-Concepción M & Vilchez D (2021) The intrinsic chaperone network of Arabidopsis stem cells confers protection against proteotoxic stress. *Aging cell* 20:e13446.

Lv B, Wei K, Hu K, Tian T, Zhang F, Yu Z, Zhang D, Su Y, Sang Y, Zhang X, *et al* (2021) MPK14-mediated auxin signaling controls lateral root development via ERF13-regulated very-long-chain fatty acid biosynthesis. *Molecular Plant* 14: 285–297

Mcswiggen DT, Mir M, Darzacq X & Tjian R (2019) Evaluating phase separation in live cells: diagnosis, caveats, and functional consequences. *Genes and Development* 33: 1619–1634

Moreno-Risueno MA, van Norman JM, Moreno A, Zhang J, Ahnert SE & Benfey PN (2010) Oscillating gene expression determines competence for periodic *Arabidopsis* root branching. *Science* 329: 1306–1311

Moreno-Risueno MA, Sozzani R, Yardımcı GG, Petricka JJ, Vernoux T, Blilou I, Alonso J, Winter CM, Ohler U, Scheres B, *et al* (2015) Transcriptional control of tissue formation throughout root development. *Science* 350: 426–430

Mruk DD & Cheng CY (2011) Enhanced chemiluminescence (ECL) for routine immunoblotting. *Spermatogenesis* 1: 121–122

Munch D, Rodriguez E, Bressendorff S, Park OK, Hofius D & Petersen M (2014) Autophagy deficiency leads to accumulation of ubiquitinated proteins, ER stress, and cell death in *Arabidopsis*. *Autophagy* 10: 1579–1587

Nolan TM, Brennan B, Yang M, Chen J, Zhang M, Li Z, Wang X, Bassham DC, Walley J & Yin Y (2017) Selective autophagy of BES1 mediated by DSK2 balances plant growth and survival. *Developmental Cell* 41: 33-46.e7

Okushima Y, Fukaki H, Onoda M, Theologis A & Tasaka M (2007) ARF7 and ARF19 regulate lateral root formation via direct activation of LBD/ASL genes in *Arabidopsis*. *Plant Cell* 19: 118–130

Orosa-Puente B, Leftley N, von Wangenheim D, Banda J, Srivastava AK, Hill K, Truskina J, Bhosale R, Morris E, Srivastava M, *et al* (2018) Root branching toward water involves posttranslational modification of transcription factor ARF7. *Science* 362: 1407–1410

Perianez-Rodriguez J, Rodriguez M, Marconi M, Bustillo-Avendaño E, Wachsman G, Sanchez-Corrionero A, de Gernier H, Cabrera J, Perez-Garcia P, Gude I, *et al* (2021) An auxin-regulable oscillatory circuit drives the root clock in *Arabidopsis*. *Science Advances* 7

Powers SK, Holehouse AS, Korasick DA, Schreiber KH, Clark NM, Jing H, Emenecker R, Han S, Tycksen E, Hwang I, *et al* (2019) Nucleo-cytoplasmic partitioning of ARF proteins controls Auxin responses in *Arabidopsis thaliana*. *Molecular Cell* 76: 177–190

Rodriguez E, Chevalier J, Olsen J, Ansbøl J, Kapousidou V, Zuo Z, Svenning S, Loefke C, Koemeda S, Drozdowskyj PS, *et al* (2020) Autophagy mediates temporary reprogramming and dedifferentiation in plant somatic cells. *The EMBO Journal* e103315

Rosado A, Li R, van de Ven W, Hsu E & Raikhel N V. (2012) *Arabidopsis* ribosomal proteins control developmental programs through translational regulation of auxin response factors. *Proceedings of the National Academy of Sciences* 109: 19537–19544

Scott RC, Schuldiner O & Neufeld TP (2004) Role and regulation of starvation-induced autophagy in the Drosophila fat body. *Developmental Cell* 7: 167–178

Sedaghatmehr M, Thirumalaikumar VP, Kamranfar I, Marmagne A, Masclaux-Daubresse C & Balazadeh S (2019) A regulatory role of autophagy for resetting the memory of heat stress in plants. *Plant, Cell & Environment* 42: 1054–1064

de Smet I, Signora L, Beeckman T, Inzé D, Foyer CH & Zhang H (2003) An abscisic acid-sensitive checkpoint in lateral root development of *Arabidopsis*. *The Plant Journal* 33: 543–555

Stephani M, Picchianti L, Gajic A, Beveridge R, Skarwan E, Hernandez VS de M, Mohseni A, Clavel M, Zeng Y, Naumann C, *et al* (2020) A cross-kingdom conserved ER-phagy receptor maintains endoplasmic reticulum homeostasis during stress. *Elife* 9: 1–105

Sugimoto K, Jiao Y & Meyerowitz EM (2010) *Arabidopsis* regeneration from multiple tissues occurs via a root development pathway. *Developmental Cell* 18: 463–471

Svenning S, Lamark T, Krause K & Johansen T (2011) Plant NBR1 is a selective autophagy substrate and a functional hybrid of the mammalian autophagic adapters NBR1 and p62/SQSTM1. *Autophagy* 7: 993–1010

Tarnowski L, Rodriguez MC, Brzywczy J, Piecho-Kabacik M, Krčkova Z, Martinec J, Wawrzynska A & Sirko A (2020) A selective autophagy cargo receptor NBR1 modulates abscisic acid signalling in *Arabidopsis* thaliana. *Scientific Reports* 10: 7778

Turco E, Savova A, Gere F, Ferrari L, Romanov J, Schuschnig M, Martens S & Savova A (2021) Reconstitution defines the roles of p62, NBR1 and TAX1BP1 in ubiquitin condensate formation and autophagy initiation. *Nature Communications* 12: 5212

Ulmasov T, Hagen G & Guilfoyle T (1997) ARF1, a transcription factor that binds to auxin response elements. *Science* 276: 1865-1868.

Wachsman G, Zhang J, Moreno-Risueno MA, Anderson CT & Benfey PN (2020) Cell wall remodeling and vesicle trafficking mediate the root clock in *Arabidopsis*. *Science (1979)* 370: 819–823

Wang HQ, Liu HM, Zhang HY, Guan Y & Du ZX (2008) Transcriptional upregulation of BAG3 upon proteasome inhibition. *Biochemical and Biophysical Research Communications* 365: 381–385

Wang S, Tiwari SB, Hagen G & Guilfoyle TJ (2005) AUXIN RESPONSE FACTOR7 restores the expression of auxin-responsive genes in mutant *Arabidopsis* leaf mesophyll protoplasts. *The Plant Cell* 17: 1979

Wang X, Jiang B, Gu L, Gu L, Chen Y, Mora M, Zhu M, Noory E, Wang Q & Lin C (2021) A photoregulatory mechanism of the circadian clock in *Arabidopsis*. *Nature Plants* 7: 1397–1408

Wang X, Yu R, Wang J, Lin Z, Han X, Deng Z, Fan L, He H, Deng XW & Chen H (2020) The asymmetric expression of SAUR genes mediated by ARF7/19 promotes the gravitropism and phototropism of plant hypocotyls. *Cell Reports* 31: 107529

Wu J, Michaeli S, Picchianti L, Dagdas Y, Galili G & Peled-Zehavi H (2021) ATI1 (ATG8-interacting protein 1) and ATI2 define a plant starvation-induced reticulophagy pathway and serve as MSBP1/MAPR5 cargo receptors. *Autophagy* 17: 3375–3388

Xie D, Chen M, Niu J, Wang L, Li Y, Fang X, Li P & Qi Y (2021) Phase separation of SERRATE drives dicing body assembly and promotes miRNA processing in *Arabidopsis*. *Nature Cell Biology* 23: 32–39

Yoshii SR, Kuma A, Akashi T, Hara T, Yamamoto A, Kurikawa Y, Itakura E, Tsukamoto S, Shitara H, Eishi Y, *et al* (2016) Systemic analysis of Atg5-null mice rescued from neonatal lethality by transgenic ATG5 expression in neurons. *Developmental Cell* 39: 116–130

Yoshimoto K, Hanaoka H, Sato S, Kato T, Tabata S, Noda T & Ohsumi Y (2004) Processing of ATG8s, ubiquitin-like proteins, and their deconjugation by ATG4s are essential for plant autophagy. *Plant Cell* 16: 2967–2983

Zhang Y, Yan L, Zhou Z, Yang P, Tian E, Zhang K, Zhao Y, Li Z, Song B, Han J, *et al* (2009) SEPA-1 mediates the specific recognition and degradation of P Granule components by autophagy in *C. elegans*. *Cell* 136: 308–321

Zhou J, Wang J, Cheng Y, Chi YJ, Fan B, Yu JQ & Chen Z (2013) NBR1-mediated selective autophagy targets insoluble ubiquitinated protein aggregates in plant stress responses. *PLoS Genetics* 9: 1004477

Zhou J, Zhang Y, Qi J, Chi Y, Fan B, Yu JQ & Chen Z (2014) E3 ubiquitin ligase CHIP and NBR1-mediated selective autophagy protect additively against proteotoxicity in plant stress Responses. *PLOS Genetics* 10: e1004116

Zuo Z, Roux M, Rodriguez E & Petersen M (2022) mRNA decapping factors LSM1 and PAT paralogs are involved in Turnip Mosaic Virus viral infection. *Molecular Plant-Microbe Interactions* 5: 125–129